RAPID COMMUNICATIONS

PHYSICAL REVIEW A VOLUME 43, NUMBER 12 15 JUNE 1991

Confined states of traveling-wave convection

C. M. Surko, Daniel R. Ohlsen, and S. Y. Yamamoto
Department of Physics and Institute for Nonlinear Science, University of California at San Diego, La Jolla, California 92093

Paul Kolodner
AT&T Bell Laboratories, Murray Hill, New Jersey 07974
(Received 23 April 1991)

Spatially confined states of traveling-wave convection of arbitrary length are studied in ethanol-water mixtures contained in a narrow annular channel, a geometry that approximates a one-dimensional system with periodic boundary conditions. The measured properties of these states, including the Rayleigh number at which they are observed, the frequency and wave number of the traveling waves, and the spatial variation of the amplitude and wave number, are in agreement with recent numerical calculations, leading to a microscopic understanding of these dynamical, nonequilibrium structures.

In convection in fluid mixtures such as ethanol and water, the onset of flow occurs as a subcritical Hopf bifurcation to states of traveling-wave convection.[1-5] In this system, a wide range of spatiotemporal behavior has been observed and studied, including states of confined traveling waves of both arbitrary[2-4] and fixed[4,5] length, in which traveling-wave (TW) convection coexists stably with conduction separated by fronts which are stationary in the laboratory frame. These confined states, which are examples of a manifest breaking of the spatial symmetry in a nonequilibrium system in the presence of a subcritical bifurcation, are analogous to the coexistence of different phases in an equilibrium system. Although there has recently been considerable theoretical attention paid to these states,[6-8] there has, until now, been no adequate microscopic understanding of these observations. Puzzling characteristics include the observed frequency, which is about a factor of 2 lower than the Hopf frequency but a factor of 5 larger than that of uniform traveling-wave states at the same Rayleigh number, and the fact that these states have fronts between conduction and convection which are stationary in the laboratory frame.

In this paper, we compare measurements of the properties of the confined states with the results of recent, finite-difference numerical calculations.[9] The calculations assume the Oberbeck-Boussinesq approximation of the fluid equations, two-dimensional flow perpendicular to the roll axes, rigid impermeable boundary conditions at the upper and lower plates of the container, and periodic boundary conditions in the other dimension. The agreement between the calculations and experiment, described in this paper, points to the microscopic mechanism by which the fronts between convection and conduction are locked in the laboratory frame. In particular, the numerical calculations[9] show that the concentration and velocity fields are phased such that there are lateral currents of concentration which steepen the concentration gradient in front of the traveling waves, thereby stabilizing this conducting region and preventing the invasion of convection. This mechanism is likely to be important in understanding other aspects of the spatiotemporal behavior observed in this and similar nonequilibrium systems.

In a binary fluid mixture, the separation ratio ψ, which is proportional to the Soret coefficient, parametrizes concentration-driven fluid density changes.[1] For $\psi<0$, the lighter component diffuses toward the colder region, thereby stabilizing the fluid layer against convection, and the Rayleigh number at onset is larger than that for a pure fluid. In this paper, all Rayleigh numbers r will be normalized by the onset Rayleigh number, R_c, of convection in a pure fluid with the same thermal properties as the mixture; thus in the mixtures studied here, $r \equiv R/R_c > 1$ above onset.

The experiments are conducted in a narrow annular channel with a rectangular cross section which provides periodic horizontal boundary conditions in the direction of the TW propagation, as in the numerical calculations. The apparatus and the properties of the fluid mixture are identical to that used in a recent study[10] of uniform states of traveling-wave convection. The convection cell has a copper bottom plate and a sapphire top plate. The vertical walls are machined plastic (ULTEM polyetherimide) of height $d=0.309\pm0.002$ cm. The cell is a narrow annulus with dimensions, in units of d, 1.288 in width by 67.09 in mean circumference. The working fluid is a mixture of 8.00% by weight ethanol in water. The top-plate temperature is set to 25.00 °C and regulated to ± 0.7 mK. Stable confined states are observed in a narrow band[2,3] of bottom-plate temperatures centered around 29.72 °C. At the confined-state Rayleigh number, the average temperature is 27.36 °C, and the fluid parameters are $\psi=-0.258$, $P=9.21$, and $L=0.008$, where the Prandtl number P and the Lewis number L are defined in the usual way.[11] The vertical thermal diffusion time, $\tau_v \equiv d^2/\kappa$, is 74.2 s, where κ is the thermal diffusivity.

The flow is visualized from above with the shadowgraph method. A two-lens, afocal optical system is used.[12] Care is taken to ensure that the intensity pattern is recorded at an axial position where the spatial modulation in the optical intensity I is in the linear regime.[13] In this case

$$I(x) \propto \int_0^1 dz \frac{\partial^2 \tilde{n}(x,t)}{\partial x^2},$$

where z is the height in the cell in units of d, x is the coor-

dinate in the annular direction, and $\tilde{n}(x,z)$ is the index of refraction modulation, which can be written

$$\tilde{n}(x,z)=a[c(x,z)+b\theta(x,z)],$$

where c and θ are the modulations in concentration and temperature fields. For the fluid described above, $b=-0.919$ using the units of c and θ given in Refs. 9 and 14.

Convection begins at a Rayleigh number $r_{co}=1.80$ with a subcritical Hopf bifurcation. This evolves to a nonlinear state of traveling waves with a frequency ω, which is approximately 45 times smaller than the Hopf frequency at the same Rayleigh number. If the Rayleigh number is then decreased, TW convection persists with ω increasing by a factor of 10 until a saddle-node bifurcation is reached at $r_s=1.62$. If the Rayleigh number is reduced below r_s, convection dies away, but not uniformly around the annulus. If the Rayleigh number is raised into a relatively narrow "locking" band in r near $r=1.68$ before convection ceases everywhere, the region or regions of TW convection that remain are found to coexist stably with regions of zero flow for arbitrarily long times.[2,3] These confined states are composed of traveling waves which are generated at one end of the convecting region and disappear at the other, with boundaries between conduction and convection which are stationary in the laboratory frame. If r is raised above (lowered below) the locking band, the spatial extent of the confined state grows (shrinks); returning r back into the band then stabilizes the state at a new length.[2,3]

Shown in Fig. 1(a) is the experimental shadowgraph intensity of a confined state as a function of position around the annulus. As time proceeds, the waves travel from left to right with a period of 83 s, while the envelope is stationary in the laboratory frame. This signal has been low-pass filtered to remove spatial frequencies above 1.7 times the fundamental. In this range of wavelengths, the signal is dominated by the temperature field $\tilde{T}(x,z)$. In order to eliminate nonuniform, time-independent contributions to the shadowgraph intensity, the data plotted at each spatial point are the intensity at one time divided by that one-half period later. For the optical contrast used in these experiments, this procedure introduces nonlinear distortions of less than 5%, but does not significantly affect the measured wavelengths. The wavelength of the waves varies markedly across the confined state. This wavelength, obtained using complex demodulation techniques,[15] is plotted as a function of position in Fig. 1(a).

Shown in Fig. 1(b) are the results of recent numerical simulations by Barten, Lücke, and Kamps[9] for the shadowgraph intensity and wavelength of a confined state which is larger in extent than that shown in Fig. 1(a) by about half a wavelength. The predicted optical signal in Fig. 1(b) has been spatially low-pass filtered in the same manner as that in Fig. 1(a). The wavelength determination procedures used in Figs. 1(a) and 1(b) were different,[9] and the lighter portions of the dashed curves correspond to shadowgraph intensities less than 20% of the maximum value, where this difference in procedure is expected to be significant. As can be seen from Fig. 1, the spatial variation of the amplitude and wavelength shown in Figs. 1(a) and 1(b) are in good agreement.

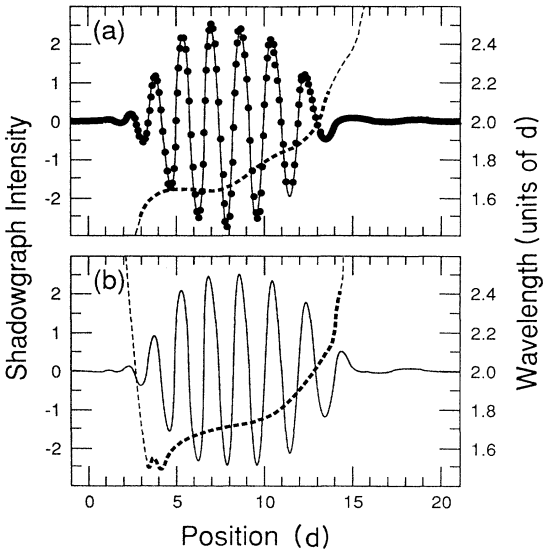

FIG. 1. Solid curves show the shadowgraph intensity as a function of position for confined states: (a) from experiment, and (b) as predicted by the numerical calculations of Ref. 9. The amplitudes have been normalized to the same arbitrary value. The waves travel from left to right. The state in (b) is longer than that in (a) by about half a wavelength, thus they are in phase on the left-hand side and 180° out of phase on the right-hand side. In (a), the data points are shown, and the curve is a guide to the eye. The dashed curves show the corresponding spatial variation of the wavelength. (See text for details.)

The parameters which characterize the confined states shown in Fig. 1 are compared in Table I. The frequency of the confined state, ω_{cf}, is a factor of 2.5 lower than the Hopf frequency ω_0 but about a factor of 5 larger than that of a uniform state at the same Rayleigh number. Experiment and the calculation for ω_{cf} agree to within about 20%. We might expect that there would be a correction due to the finite transverse aspect ratio in the experiment as compared to the infinite, two-dimensional assumptions of the calculation which would affect ω_{cf} and ω_0 in a similar way. When we normalize ω_{cf} by ω_0, excellent agree-

TABLE I. Parameters that characterize the confined states shown in Figs. 1(a) and 1(b) are compared. The wavelength λ_{cf} and the index of refraction modulation $\tilde{n}_{cf}$ are evaluated at the position at which the amplitude is a maximum.

Confined state parameter	Experiment	Numerical calculation (Ref. 9)
ω_{cf} (units of rad/τ_v)	5.58 ± 0.07	4.53
ω_{cf}/ω_0	0.404 ± 0.005	0.403
λ_{cf}/d	1.68	1.72
$\tilde{n}_{cf}/\tilde{n}_u$	0.74	0.85
r_{cf}	1.68	1.25
r_s	1.62	1.21
$\frac{r_{cf}-r_s}{r_{co}-r_s}$	0.33	0.26

ment between the experiment and the calculations is found. Similarly, the measured index of refraction modulation in the confined state, $\tilde{n}_{cf}$, normalized by that for a uniform state at the same Rayleigh number, $\tilde{n}_u$, is in good agreement with the results of the numerical calculations, as is the wavelength λ_{cf}/d at maximum amplitude. Comparison of the Rayleigh number r_{cf} where the confined states are observed appears to show a similar effect. The absolute comparison is 1.68 for the experiment and 1.25 in the calculation, but when the fractional distance in Rayleigh numbers between the confined state and the saddle node, $r_{cf}-r_s$, is compared with the distance between the saddle node and the onset of the oscillatory instability, $r_{co}-r_s$, better agreement is obtained (see Table I).

The one prediction of the numerical calculations which disagrees with our experiments is the observation that, experimentally, the confined states are stationary in the laboratory frame, but in the calculations they move with a group velocity which is small but nonzero— $\frac{1}{70}$ of the phase velocity obtained using the Hopf frequency (i.e., about $\frac{1}{30}$ of the phase velocity of the waves in the confined states). It is possible that this discrepancy is due to the finite transverse aspect ratio of the experimental geometry as compared with the infinite, two-dimensional assumptions of the calculations.[9] This point warrants further consideration.

Confined states of arbitrary spatial extent, consisting of traveling waves propagating in either direction, can be obtained at arbitrary positions in the annulus. Shown in Fig. 2 are experimental data for the envelopes of the shadowgraph intensity of four confined states of different sizes, at the same Rayleigh number. Also shown in Fig. 2 are corresponding plots of the wavelength as a function of position. (In comparing Figs. 1 and 2, d is equal to 5.37°.) The envelopes and wavelengths shown were obtained by complex demodulation, as described in Ref. 15. Figure 2(b) is the same state as that shown in Fig. 1(a); and Fig. 2(a) has been reversed so that, in the figure, the waves in all four states travel from left to right. These states were obtained in different experimental runs and have been translated in absolute position [by (a) 110°, (b) 30°, (c) 7.5°, and (d) −72°], so they are roughly centered at 180° in the figure. Qualitatively, both the amplitude and wavelength are constant in the interior of the confined state and vary rapidly only near the ends.[16] The maximum amplitudes of all states are similar, and the frequencies of all states are the same to within the error bars quoted in Table I. Similar behavior as a function of size was reported for the two confined states observed in the numerical calculations[9] at this value of ψ.

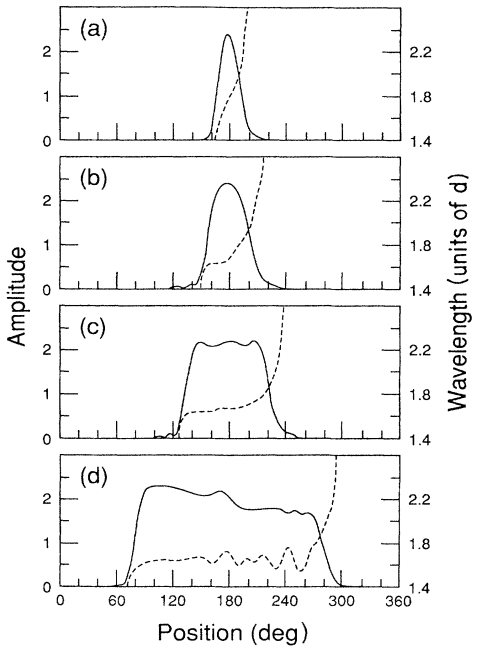

FIG. 2. Shown are the envelopes of the experimental shadowgraph intensity and the corresponding wavelengths of confined states of various sizes. The amplitudes have been normalized to the same arbitrary value. The waves travel from left to right. (See text for details.)

The shape of the envelope of the confined states is also similar to the predictions of Ref. 9. The amplitudes of the velocity and temperature fields, shown in Ref. 9, increase toward the leading edge of the confined states, but the shadowgraph images are weighted by λ^{-2}, where λ is the local wavelength. This factor makes the shadowgraph intensity larger near the trailing edge, as is observed in our experiments.

The measurements described here and the calculations described in Ref. 9 point out the similarity of these states of arbitrary length, to those described in Refs. 4 and 5, which were observed in a different parameter regime (i.e., $\psi \simeq -0.08$). These latter states were observed to be fixed in length and of a size similar to the state shown in Fig. 2(a). In both cases, there is a similar and marked change in wavelength across the convecting region,[4,5,9] and the frequencies of these states, relative to the Hopf frequency, are also very similar. The mechanism for confinement is likely the same for the states discussed here and those described in Refs. 4 and 5.[9]

In this paper, we have described a quantitative comparison between recent two-dimensional numerical calculations of the fluid equations and experimental measurements of confined TW states of arbitrary length. The frequency, amplitude, wavelength, and spatial variation of the wavelength in the confined states are in good agreement, even though most of these quantities are distinctly different than those for either uniform linear or fully developed nonlinear states of traveling-wave convection. This agreement gives us confidence in examining the most puzzling aspect of the confined states, which is the mechanism by which these states are locked, or, in the case of the calculations, move slowly in the laboratory frame. The answer[9] is that the phasing of the time-dependent concentration and velocity fields produces lateral, dc concentration currents which result in the steepening of the concentration gradient in front of the confined state, thereby stabilizing this region with respect to the invasion of traveling-wave convection. Thus this stabilization mechanism is an intrinsically dynamical phenomenon.

The agreement between the calculations and experi-

ment for these confined states gives us hope that, by the combination of numerical calculations and laboratory experiments, we can achieve a detailed understanding of the other spatiotemporal phenomena[2–5] observed in this dynamical, nonequilibrium system. The results described above may also provide insight into the minimum amount of complexity required for a reduced (e.g., a model equation) description of these phenomena.

We are grateful to W. Barten and M. Lücke for many helpful conversations and for providing us with the results of their numerical calculations, and we wish to acknowledge the technical assistance of K. D. Eaton and H. L. Williams. This work was supported by the Department of Energy under Grant. No. DE-FG03-90ER14148 and the Defense Advanced Research Projects Agency University Research Initiative Contract No. N00014-86-K-0758.

[1]P. Kolodner, C. M. Surko, and H. Williams, Physica D **37**, 319 (1989), and references therein; R. Heinrichs, G. Ahlers, and D. S. Cannell, Phys. Rev. A **35**, 2761 (1987); E. Moses, J. Fineberg, and V. Steinberg, *ibid.* **35**, 2757 (1987).

[2]P. Kolodner, D. Bensimon, and C. M. Surko, Phys. Rev. Lett. **60**, 1723 (1988).

[3]D. Bensimon, P. Kolodner, and C. M. Surko, J. Fluid Mech. **217**, 441 (1990).

[4]K. E. Anderson and R. P. Behringer, Phys. Lett. A **145**, 323 (1990).

[5]J. J. Niemela, G. Ahlers, and D. S. Cannell, Phys. Rev. Lett. **64**, 1365 (1990).

[6]D. Bensimon, B. I. Shraiman, and V. Croquette, Phys. Rev. A **38**, 5461 (1988).

[7]S. Fauve and O. Thual, Phys. Rev. Lett. **64**, 282 (1990).

[8]W. van Saarloos and P. C. Hohenberg, Phys. Rev. Lett. **64**, 749 (1990), and references therein.

[9]W. Barten, M. Lücke, and M. Kamps, Phys. Rev. Lett. **66**, 2621 (1991).

[10]D. R. Ohlsen, S. Y. Yamamoto, C. M. Surko, and P. Kolodner, Phys. Rev. Lett. **65**, 1431 (1990).

[11]P. Kolodner, H. Williams, and C. Moe, J. Chem. Phys. **88**, 6512 (1988).

[12]V. Croquette, Contemp. Phys. **30**, 113 (1988).

[13]S. Rasenat, G. Hartung, B. L. Winkler, and I. Rehberg, Exp. Fluids **7**, 412 (1989).

[14]W. Barten, M. Lücke, W. Hort, and M. Kamps, Phys. Rev. Lett. **63**, 376 (1989); W. Barten, M. Lücke, and M. Kamps, in *Nonlinear Evolution of Spatio-Temporal Structures,* edited by F. H. Busse and L. Kramer, NATO Advanced Study Institutes Ser. B2 Vol. 225 (Plenum, New York, 1990), p. 131.

[15]P. Kolodner and H. Williams, in *Non-Linear Evolution of Spatiotemporal Structures* (Ref. 14), p. 73.

[16]The variation in amplitude and wavelength in Fig. 4(d) between 160° and 250° may be due to optical distortions.